# Low-Cost Accelerometers for Experimental Modal Analysis

**S. Beskhyroun & Q. Ma**
*The University of Auckland, Auckland, New Zealand*

**SUMMARY:**
The application of Micro-electro-mechanical system (MEMS) based accelerometers has increased exponentially in recent years. It has also experienced an increase in popularity in the structural testing community as they are economical and accurate over large frequency range. Despite the obvious advantages, reservations of using these devices still exist amongst researchers as they are relatively untested. This paper summarises the operating requirements and preferences for using such accelerometers for structural experimental modal analysis. The challenges for adapting MEMS based devices are discussed. The paper presents an interesting example of the application of MEMS based accelerometer for experimental modal analysis of a high rise reinforced concrete building subjected to a series of strong aftershocks. The extracted modal data demonstrated comprehensively that the perceived inaccuracies when using MEMS based devices are in fact well within the standard errors in experiments conducted in a conventional manner.

*Keywords: Experimental modal analysis, MEMS Accelerometer, Earthquake engineering*

## 1. INTRODUCTION

The identification of dynamic characteristics such as natural frequencies, mode shapes, and modal damping is a necessary and important task in the course of seismic design of civil engineering structures [Farrar, C. R. and James, G. H. 1997]. To accomplish this task, researchers commonly carry out ambient vibration tests, forced vibration tests, free vibration tests, and earthquake response measurements. Among these field tests, ambient vibration experiments are most common place as they are economical, non-destructive, fast and easy to conduct. However, as the input in ambient vibration tests is usually weak, these tests are not so effective in obtaining accurate estimation of the higher modes data and uncertainties remain on whether the modal information would apply to different strain ranges. Forced vibration tests overcome these issues by providing higher input forces. However, they are substantially more expensive, time consuming to conduct and often require special permissions as there is an increased likelihood of damaging the structure. Earthquake response measurement is simply a form of structural monitoring during earthquake events. This is particularly advantageous for earthquake engineering research purposes as the excitation occurs naturally and is the most realistic. Unless instrumentation is implemented on structures on a continuous basis, typically only a small window of opportunity exists to install these arrays of sensors in time for any aftershock sequence. The successful implementation of large sensing networks is limited by the high cost of installing and maintaining the extensive lengths of wiring needed in a large civil structure to connect individual sensors to a central repository [Çelebi, M. 2002]. As a result of these high costs and difficulties, the use of MEMS based accelerometers is an attractive economical alternative. As these accelerometers generally have low power consumption, they can often operate for an extended period only powered by a battery. Moreover, some battery operated MEMS accelerometers have the analogue-to-digital conversion and data recording capability built in, further simplifying the set up and permits a far more locations to be monitored than usual. This paper presents the application of low-cost MEMS accelerometers to a number of damaged buildings in the Christchurch central business district (CBD), New Zealand after two major earthquakes; a magnitude 7.1 event on September 4, 2010 and a more damaging magnitude 6.3 event on February 22, 2011. The accelerometers captured very high quality building response data as the buildings experienced thousands of aftershocks. The challenges for adapting MEMS based devices for successful modal parameters identification are also discussed.

## 2. MICRO-ELECTRO-MECHANICAL SYSTEM (MEMS) BASED ACCELEROMETERS

### 2.1. Description and usage issues

MEMS based accelerometer sensors are now widely used in many recent developments and applications. This includes the aerospace, automotive, computer manufacturing and home entertainment industries. In this project, USB accelerometers X6-1A (Fig. 2.1) produced by the Gulf Coast Data Concepts were selected to measure the response of three reinforced concrete buildings subjected to earthquake excitation. A quantitative analysis of the accuracy of this accelerometer can be found in a paper by [Haritos, N. 2009].

The price of each accelerometer as of 2011 was US$90. The heart of the X6-1A accelerometer is a low noise digital 3-axis MEMS accelerometer chip by STMicroelectronics. The X6-1A stores the precise time stamped data on microSD memory and it is also possible to access the real-time data via USB connectivity. Acceleration in X, Y, and Z axes are measured and stored at a user selectable rate of up to 320Hz. The STMicroelectronics MEMS sensor incorporates over sampling and anti-aliasing, and the real time data is streamed digitally via a I2C bus. An 8bit Silicon Labs 8051 microprocessor collects the data, processes the stream and is logged to the microSD card. The advantage of this set up is that it requires no additional analogue-to-digital conversion.

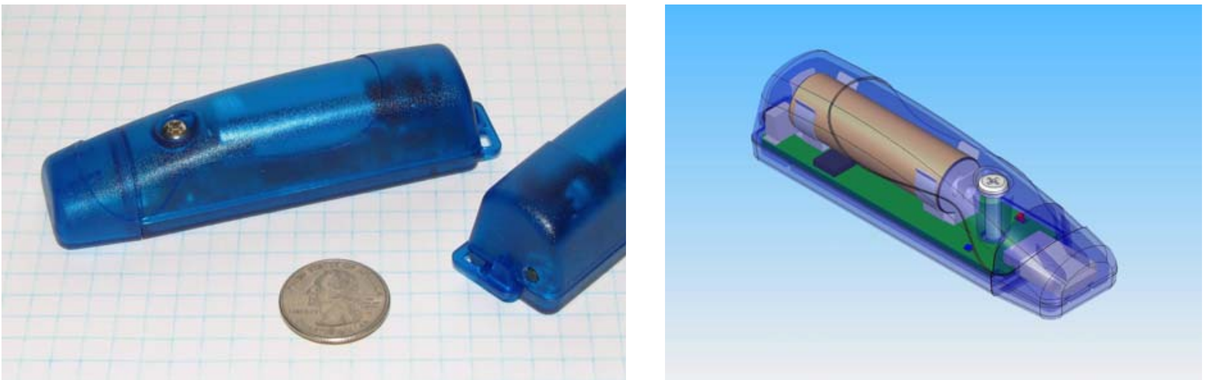

**Figure 2.1.** Accelerometer X6-1A

### 2.2. Battery consumption

The X6-1A accelerometer is normally powered by a single "AA" sized battery. According to the manufacturer, typical operation time using an alkaline battery ranges from 3 to 7 days depending on system configuration, battery quality and microSD card type. However, in our first test setup the AA battery lasted for only 20 hours, which restricted the amount of data collected in first building. Consequently, modifications were made to the accelerometers to use a D-cell battery (Fig. 2.2) which increased their typical battery life to around three weeks. It was noted that the battery consumption was influenced significantly by the micro-resolution settings. When micro-resolution was activated, the microprocessor operated at full speed at all times to ensure the timing accuracy is maintained within 1 μs, this reduced the operating life significantly. When micro-resolution is deactivated, the time resolution is approximately 1 ms. In this project, it was decided to turn the micro-resolution off as it was more important to extend the battery life to increase the chance of recording more aftershocks and, moreover, 1 ms time resolution was considered sufficiently accurate for our application.

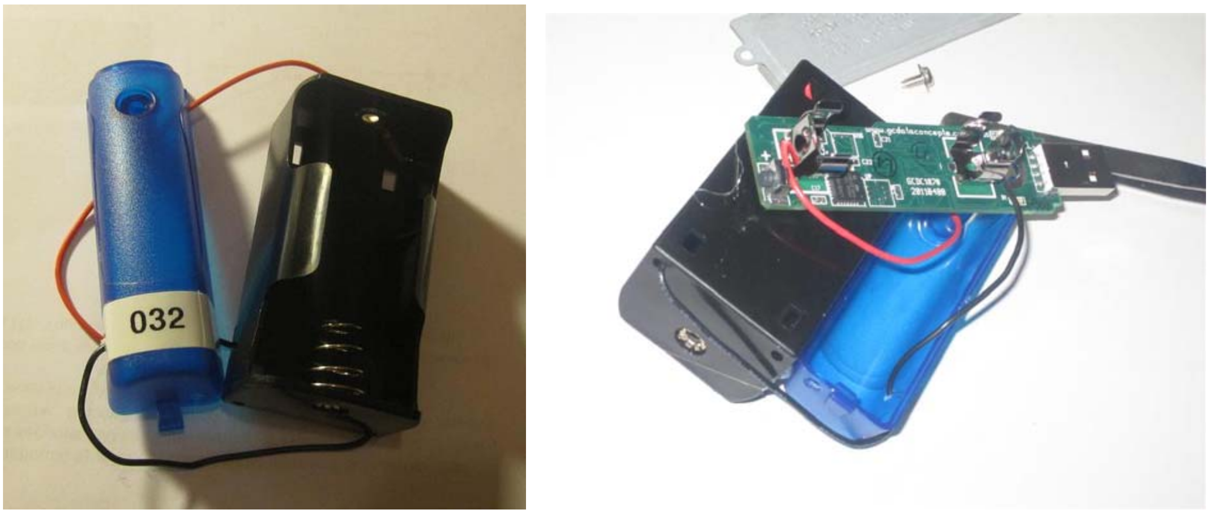


**Figure 2.2.** Accelerometer X6-1A equipped with a D-cell battery holder

### 2.3. Drift in real time clock (RTC)

A real time clock (RTC) chip, DS3231 from Maxim/Dallas Semiconductor controls the timing of the X6-1A. It determines the time stamp for each line of data recorded. Initializing the RTC ensures that the start time and individual time stamps can be correlated to an absolute time. Direct initialization of the RTC is possible but requires specific device drivers from Gulf Coast Data Concepts. The RTC maintains ±2ppm accuracy (0°C to +40°C) and is backed up by a separate power system when the battery is not present or when the device is not attached to USB power supply. The RTC can operate for about 12 hours using the backup power. The RTC also provides the system temperature (°C) which is recorded to the header of each data file.

Before installation of the accelerometers into the monitored buildings, the RTC of the accelerometers are synchronised to a computer clock. Experiments have shown that this approach produces exact synchronisation of the RTC in different accelerometers immediately after initialising the clock. However, as time elapses, a small drift of the RTC in the different units can be noticed, causing a time lag between the accelerometers. This drift in the RTC clock would lead to inaccurate phase angle data between the accelerometers causing errors in mode shapes and producing distorted results. Natural frequencies and modal damping parameters are not influenced by this issue, as they can be estimated from a single accelerometer. To overcome this issue, the following two post-processing approaches were proposed.

In the first method, at the end of each test setup, the accelerometers were placed on a rigid plate which was shaken manually to produce a cyclic graph. Keeping one accelerometer as a reference, the acceleration time histories of other accelerometers were manually shifted to maximise the correlation. This shift was then used to calculate a drift per unit time and applied linearly to correct the time difference between each accelerometer and a reference. Fig. 2.3 shows an example of a time lag between two accelerometers after about three weeks from initialising the RTC. Although this method appears simplistic, it has been shown to produce very accurate relative RTC drift estimate between different accelerometers.

In the second method, the first mode natural frequency is first estimated using the Peak Picking (PP) method [Bendat, J. S. and Piersol, A. G. 1993]. Then the Cross Spectrum Density (CSD) between each accelerometer and a reference accelerometer is estimated. The phase angle at different frequencies can be obtained from the CSD data. In the first bending mode, all points of the building are supposed to be in-phase and hence the phase angle between any accelerometer and the reference should be zero. Any phase angle value of the first bending mode different from zero is assumed to be due to the drift in the RTC. Given the frequency of the first mode and the phase angle difference, the time lag can be estimated from the following formula:

$$\delta t = \frac{difference\,in\,phase\,angle\,(in\,radians)}{f \times 2\pi} \tag{2.1}$$

where $f$ is the natural frequency of the first mode in Hertz.

Another complication arises from the fact that over time, the lag between two accelerometers can be greater than one cycle of the first mode ($1/f$). This was easier to deal with when using the first method, because it can be identified by inspection. For the second method, even if the phase difference was greater than one cycle, only the remaining angle was determinable. Since the effects of time lag only becomes more prominent with time, the first few aftershocks logged by the accelerometer were used to identify mode shapes. This ensured a lower possibility of having a time delay greater than one cycle. It is therefore recommended to use the second method in conjunction with the first to overcome the time lag in RTC more efficiently.

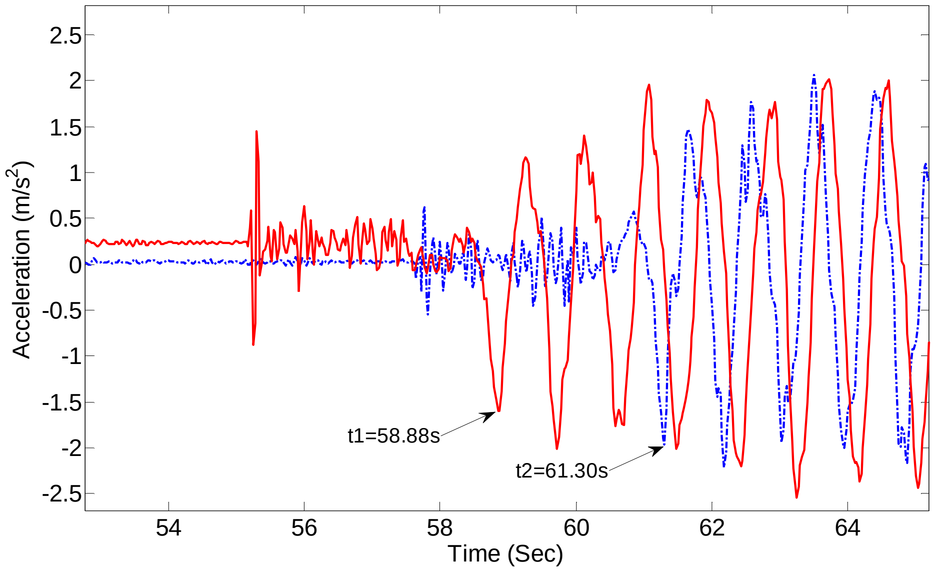


**Figure 2.3.** Time lag between two accelerometers after about three weeks from initialising the RTC

## 2.4. Delay in data acquisition and fluctuation of the sampling rate

Recorded acceleration data is written to files in comma separated text format starting with the file header information and followed by data entries. The header describes the system configuration, firmware version, and the precise time when the file was created. Data entries include a time stamp and the raw accelerometer sensor readings from the X, Y, and Z axes. The time stamp is seconds elapsed from the start time in the header. The raw sensor data format is signed digital "counts". Occasionally, there is a delay in data acquisition due to extended read/write operations to the microSD card. This occurs when the system needs to find and allocate a new cluster in the flash memory. The time needed to complete this task sometimes exceeds the cache buffer so the data is dropped. However, time stamps are always absolute based on input from the real time clock. Therefore, resampling the data from multiple units to time align the samples is required. Resampling is also important to ensure that the time intervals agree between devices. The X6-1A records data as it is streamed from the accelerometer sensor. The sensor streams data based on the timing of an internal clock (not the RTC). This sensor clock is not perfect and the precision and drift are undefined. For example, a selected sample rate of 40 Hz may actually fluctuate around this value, as shown in Fig. 2.4, which will result in non-constant time interval between consecutive data records. The precise RTC of the data loggers is used to independently time stamp the sensor data. Data from multiple units will align properly when each data set is resampled to the same frequency. A spline function was used to resample the data.

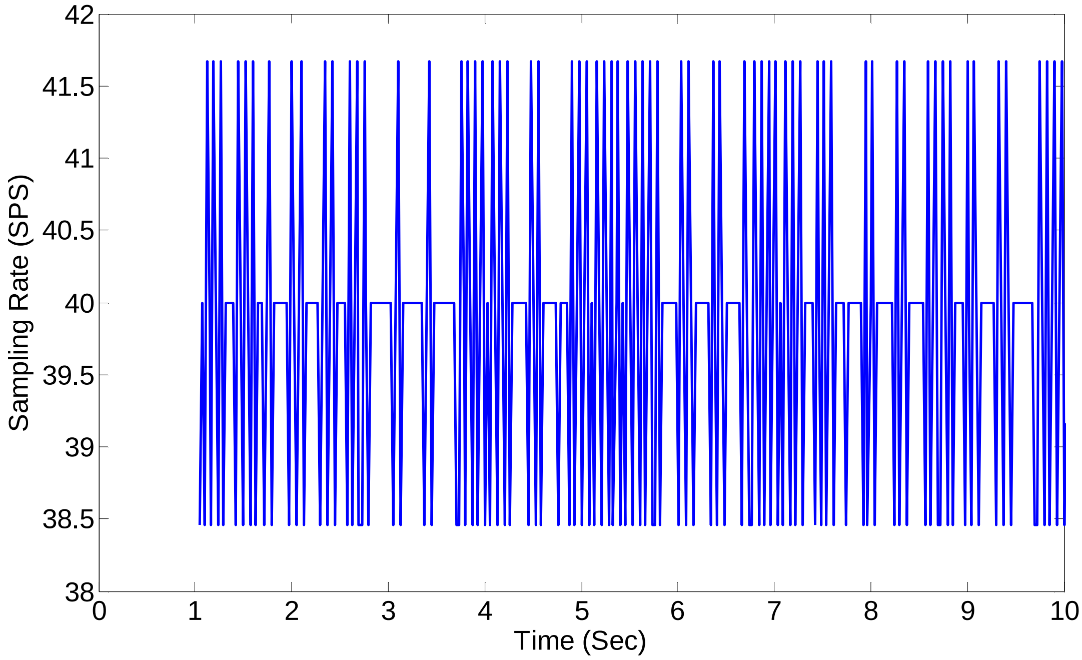


**Figure 2.4.** Fluctuation of the sampling rate

### 2.5. Continuous data recording

Since the accelerometers record data continuously once they are turned on until the end of the test (about three weeks), it was necessary to crop the acceleration data at the aftershock time and discard other data. Detailed information about earthquakes and aftershocks in New Zealand were obtained from the GeoNet website (http://www.geonet.org.nz). This information included time, magnitude and location of the aftershocks. A MATLAB [Mathworks 2010] program was developed to crop the data collected by each accelerometer to the duration of the aftershock as obtained from GeoNet. The program resamples the data and converts raw acceleration data from "counts" to $ms^{-2}$. The crop software also synchronizes data from different accelerometers as described in the previous section. These cropped files are text files, containing the data merged from all the accelerometers, with the header containing the starting and ending time of the crop. Acceleration data in X, Y and Z directions are saved in separate files.

## 3. INSTRUMENTED BUILDINDS

After the two major earthquakes in Christchurch city, New Zealand in September 2010 and February 2011, several buildings in the CBD were red stickered, cordoned and became inaccessible to general public due to the intensity of the damage they experienced. Some of these buildings have already been demolished while the fate of some others is still unknown. A group of researchers from the Civil and Environmental Department in the University of Auckland were granted permission to enter the red zone and instrument three reinforced concrete buildings with a large number of MEMS based accelerometers. The accelerometers were placed in the buildings between late July and early November of 2011. Out of these three buildings, the most severely damaged building was a 17 storey structure with plan dimensions of 35m by 25m. It was instrumented twice with 15 and 18 accelerometers respectively. Unfortunately, only a few sizable aftershocks were recorded from these setups due to issues with the accelerometer battery. The second instrumented building was a 12 storey building with plan dimensions of 31m by 23.2m attached to a 2 storey car park. The third building was a 14 storey building. These two buildings had about 20 to 30 accelerometers deployed in each building that recorded many high quality aftershocks. A typical acceleration response and the corresponding power spectral density (PSD) at the 12$^{th}$ floor from a 3.8 Richter magnitude aftershock is depicted in Figs. 3.1. (a) and (b), respectively.

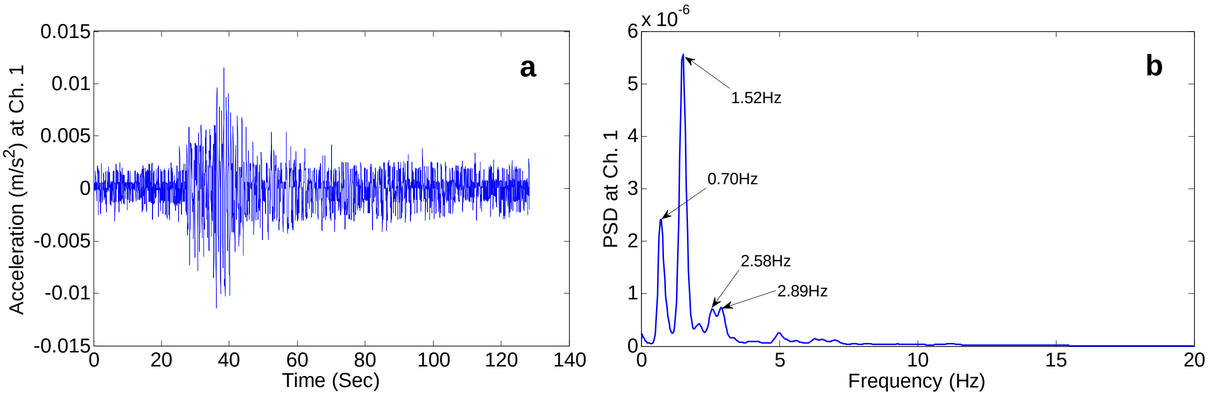


**Figure 3.1.** (a) Typical acceleration response and (b) the corresponding PSD at the 12th floor from a 3.8 Richter magnitude aftershock

## 4. RESULTS

### 4.1. Natural frequencies

The natural frequencies estimates from the recordings made during each aftershock were found using the PSD function. These were manually recorded onto a spreadsheet with the aftershock information. Table 4.1 shows a sample of the natural frequencies obtained from the second building.

**Table 4.1.** Natural frequencies recorded from PSD function

| Aftershock Details | Natural Frequencies (Hz) | | | | |
|---|---|---|---|---|---|
| | F1 | F2 | F3 | F4 | F5 |
| **NZ Standard Time: Thursday, 25 August 2011 at 9:33 am**<br>Latitude, Longitude: 43.59º S, 172.93ºE<br>Location: 20km East of Lyttelton<br>Focal depth: 9 km<br>Richter magnitude: 3.8 | 0.703 | 1.484 | 2.617 | 2.890 | 4.999 |
| **NZ Standard Time: Friday, 26 August 2011 at 7:46 pm**<br>Latitude, Longitude: 43.50º S, 172.70ºE<br>Location: 10km North-East of Christchurch<br>Focal depth: 7 km<br>Richter magnitude: 2.7 | 0.742 | 1.601 | 2.499 | 3.085 | 5.155 |

### 4.2. Mode shapes

Table 4.2 shows the accelerometers locations in the second building marked by normal font. As indicated in this table, some corners were not instrumented due to the limited number of available accelerometers. To achieve accurate and smooth mode shapes, some assumptions were made to fill in missing data. Referring to Fig. 4.1 and considering the acceleration in X-direction (East), it was assumed that the acceleration in the North-West and North-East corners are equal due to the in-plane rigidity of the floors and likewise for the South-West to South-East corners. Similarly, for the Y-direction (North), the accelerations in the North-West and South-West corners, and South-East and North-East corners were assumed to be equal. In Table 4.2 marked in bold are the accelerometer data that has been taken from another corner according to assumptions made for the X-axis. For the building levels which had no accelerometers, such as levels 5 and 8, interpolation between modal amplitudes in each corner was carried out using cubic polynomial to obtain modal amplitudes at these levels. A MATLAB based program [Beskhyroun, S. 2011], developed in the University of Auckland, was utilized for modal parameters identification. The simple peak picking (PP) method in frequency domain and the more advanced stochastic subspace identification (SSI) method in time domain [Overschee, P. van and Moor, B. D. 1996 & Katayama, T. 2005] were adopted to extract modal data. Two techniques were implemented to find stable poles in the SSI method. In both techniques the algorithm starts with a high system order which is then reduced by two with each iteration until the final iteration was run with a system order of two. Stable poles identified in each of these iterations were compared by one of two techniques. In the first technique (SSI1), the stable poles identified around the singular values generated from the singular value decomposition of the power spectral density matrix [Brincker, et al. 2000], were compared. If two consecutive poles within ±“SVD_dF” Hz of the singular value had change in frequencies within (Freq%), change in damping within “Damp%” and a modal assurance criteria (MAC) [Ewins, D.J. 2000] value greater than “MAC” user defined values, both poles were kept and averaged. If both poles did not meet these criteria the first pole was discarded and the second pole was compared to the subsequent one. This series of comparisons was continued until all stable poles in the frequency range had been compared and averaged. The resulting mode shape, natural frequency and damping are the combination of several stable poles and therefore provided a robust method of system identification. While the first technique used singular value decomposition of the PSD matrix to identify stable poles, the second one (SSI2) breaks up the entire frequency range tested into “SSI2_dF” Hz bands. Those bands with the most poles are considered to contain true modes and are then used to get stable modes. Stable poles are found within each band and averaged using the same procedures as in the previous SSI1 technique.

Figs. 4.2 to 4.5 show four mode shapes identified by the PP method of the second building when excited by a magnitude 3.8 aftershock. It is clearly indicated in these figures that the high quality acceleration data captured by the accelerometers together with the implemented solutions has resulted in a very accurate identification of mode shapes even for the higher modes.
The modal assurance criterion (MAC) is generally used as a measure of the correlation between two mode shapes. For the current study, the MAC value was used to compare mode shapes from various system identification methods. The MAC value corresponding to the $i^{th}$ mode shapes, $\boldsymbol{\phi}_i$ and $\boldsymbol{\phi}_i$*, is defined as

$$MAC_i = \frac{\left[\sum_{j=1}^{n} \phi_{ij}\phi_{ij}^{*}\right]^2}{\sum_{j=1}^{n}\phi_{ij}^2 \sum_{j=1}^{n}\phi_{ij}^{*2}} \tag{4.1}$$

**Table 4.2.** Location of accelerometers in the second building.

| Level | Accelerometer ID in corner | | | |
|---|---|---|---|---|
| | NE | SE | SW | NW |
| G | 015 | 009 | 002 | **015** |
| 1 | 022 | **016** | 016 | **022** |
| 2 | 011 | 039 | 021 | 055 |
| 3 | 012 | **006** | 006 | **012** |
| 4 | **044** | 031 | **031** | 044 |
| 5 | | | | |
| 6 | **005** | 008 | **008** | 005 |
| 7 | 014 | **013** | 013 | **014** |
| 8 | | | | |
| 9 | 020 | **036** | 036 | **020** |
| 10 | 004 | 003 | 060 | 001 |
| 11 | 054 | 051 | **051** | **054** |

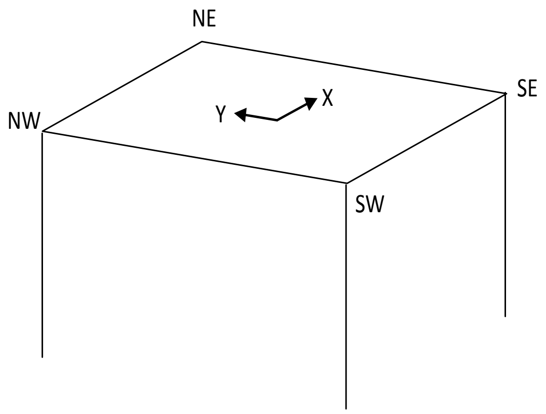


**Figure 4.1.** Axes of the second building

where $n$ is the number of elements in the mode shape vectors. A MAC value close to unity indicates perfect correlation between the two shapes and values close to zero indicate shapes that are orthogonal. Figs. 4.6 to 4.9 show MAC values for four mode shapes identified by PP, SSI1 and SSI2 methods. Each bar in these figures represents the MAC value when comparing one specific mode extracted from a pair of system identification methods. MAC values ranged from 0.80 to 1.00 which indicated a very high correlation between mode shapes identified by the different system identification methods. A near perfect correlation was noticed for the first bending mode, the first torsional mode and the second torsional mode.

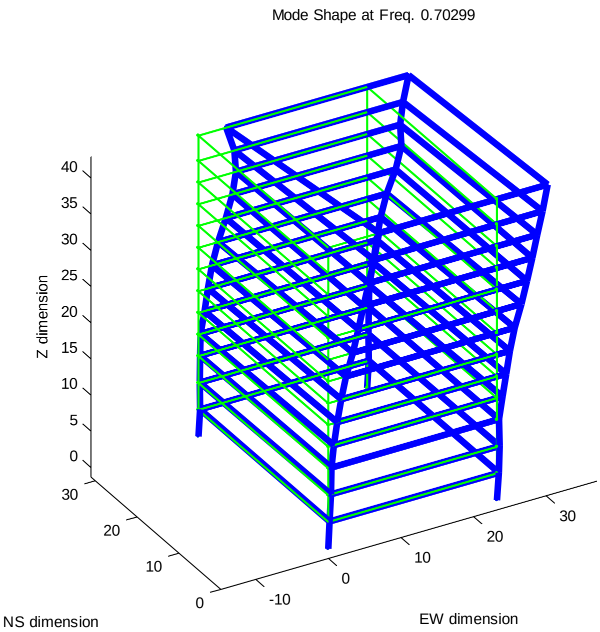


**Figure 4.2.** Mode shape of the first bending mode

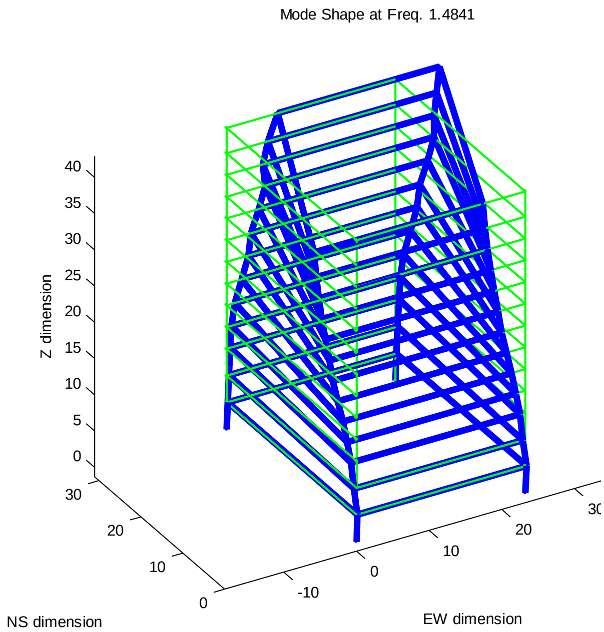


**Figure 4.3.** Mode shape of the first torsional mode

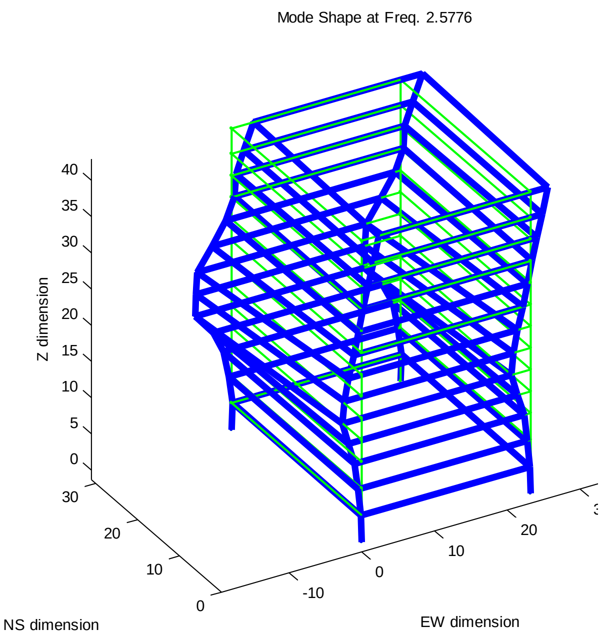


**Figure 4.4.** Mode shape of the second bending mode

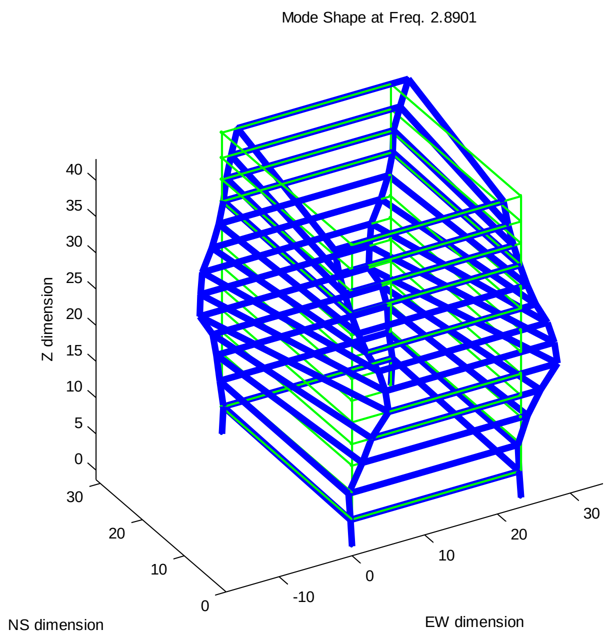


**Figure 4.5.** Mode shape of the second torsional mode

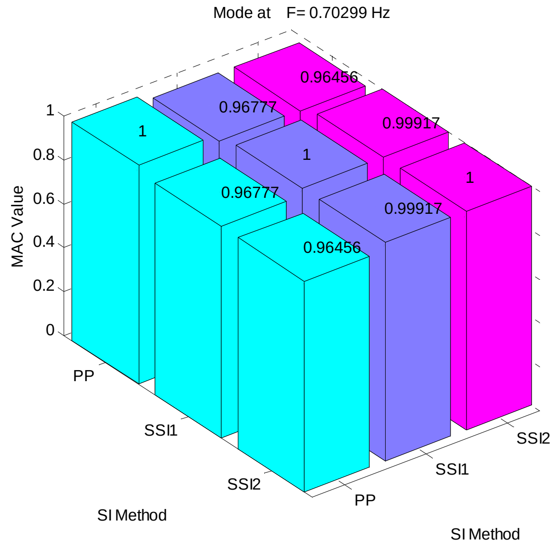


**Figure 4.6.** MAC values for the first bending mode

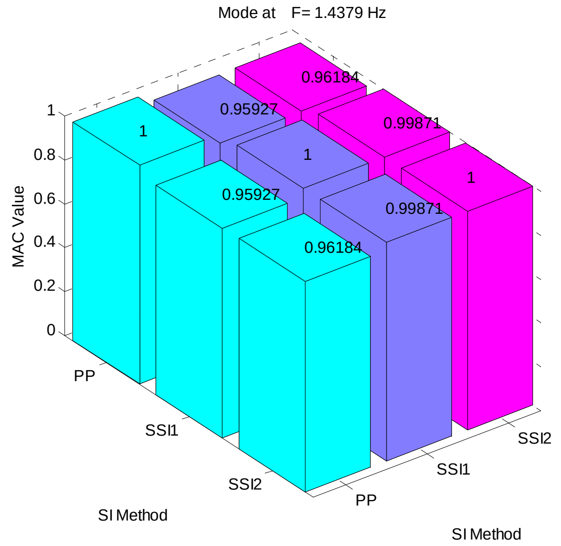


**Figure 4.7.** MAC values for the first torsional mode

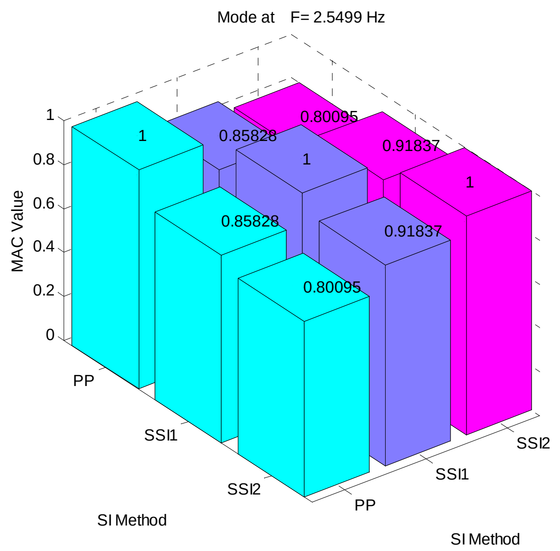


**Figure 4.8.** MAC values for the second bending mode

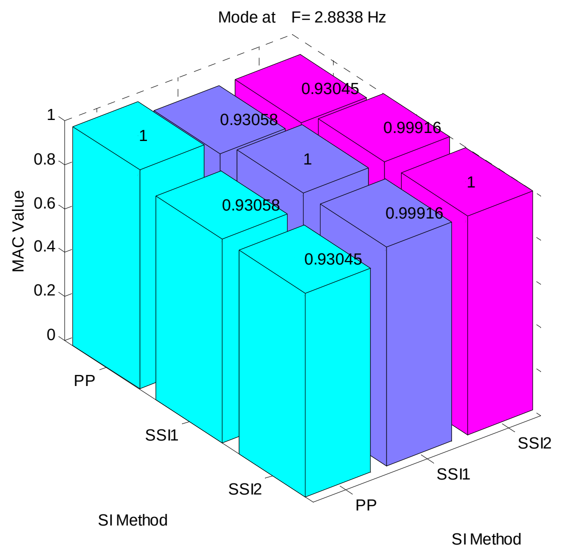


**Figure 4.9.** MAC values for the second torsional mode

## 4.3. Damping

Table 4.3 summarizes the natural frequencies and the corresponding damping values as identified by SSI1 and SSI2 methods.

**Table 4.3.** Natural frequencies and damping values

| **Mode shape** | **SSI1** | | **SSI2** | | **PP** |
|---|---|---|---|---|---|
| | Frequency (Hz) | Damping (%) | Frequency (Hz) | Damping (%) | Frequency (Hz) |
| First bending | **0.76** | 1.47 | **0.81** | 1.48 | **0.70** |
| First torsional | **1.44** | 3.74 | **1.45** | 3.92 | **1.48** |
| Second bending | **2.55** | 2.24 | **2.55** | 2.23 | **2.66** |
| Second torsional | **2.88** | 2.99 | **2.89** | 3.02 | **2.89** |

## 5. CONCLUSIONS

The successful application of low-cost MEMS accelerometers for the identification of modal parameters of civil engineering structures has been investigated in this paper. A dense array of MEMS accelerometers were successfully utilized to record several aftershocks response of three high rise reinforced concrete buildings in Christchurch city, New Zealand after the city with hit by two major earthquakes. The recorded data produced very accurate estimates of the modal parameters of the instrumented buildings. Two commonly used system identification techniques, the frequency domain peak pick method and the more advanced time domain stochastic subspace identification method were implemented to extract modal parameters. Very high correlation between modal parameters from the two methods was found.

The paper also demonstrated a number of techniques to overcome issues with the accelerometers such as the short battery life, the drift in the RTC, the delay in data acquisition and the fluctuation of the sampling rate in the internal data logging system.

**AKCNOWLEDGEMENT**
The financial support of the New Zealand Earthquake Commission (EQC) is gratefully acknowledged. The authors are very thankful to Prof. Barry J. Davidson, Mr. Roger Brown, Mr. Anthony McBride and Dr. Nicholas Brooke from Compusoft Engineering LTD for their technical and logistic support. Special thanks to Banurathy Sivanantharajah, summer research student for her assistance in preparing the recorded data.

**REFERENCES**

Bendat, J. S. and Piersol, A. G. (1993). Engineering Applications of Correlation and Spectral Analysis, *New York, Wiley*.

Beskhyroun, S. (2011). Graphical interface toolbox for modal analysis. *Proceedings of the Ninth Pacific Conference on Earthquake Engineering*, Auckland, New Zealand.

Brincker, R., Zhang, L. and Andersen, P. (2000). Modal Identification from Ambient Responses using Frequency Domain Decomposition, *Proceedings of the 18$^{th}$ International Modal Analysis Conference (IMAC)*,USA.

Çelebi, M. (2002). Seismic Instrumentation of Buildings (with Emphasis on Federal Buildings). **Report No. 0-7460-68170**, United States Geological Survey, Menlo Park, CA

Ewins, D.J. (2000). Modal Testing: Theory, Practice and Applications, *2$^{nd}$ Edition, Research Studies Press Ltd*., Hertfordshire, England.

Farrar, C. R. and James, G. H. (1997). System identification from ambient vibration measurements on a bridge, *Journal of Sound and Vibration*, **205(1): 1−18**.

Haritos, N. (2009). Low Cost Accelerometer Sensors - Applications and Challenges. *Australian Earthquake Engineering Society 2009 Conference*, Newcastle, Australia.

MATLAB 2011a. (2011). *The MathWorks Inc*., Natick, MA.

Overschee, P. van and Moor, B. D. (1996). Subspace Identification for Linear Systems, *Kluwer Academic Publishers*.

Katayama, T. (2005). Subspace Methods for System Identification, *Springer*.